ACS APPLIED BIO MATERIALS

www.acsabm.org

Article

Graphene-Based Field-Effect Transistor for Ultrasensitive Immunosensing of SARS-CoV-2 Spike S1 Antigen

Deepshikha Shahdeo,[⊥] Neha Chauhan,[⊥] Aniket Majumdar, Arindam Ghosh,* and Sonu Gandhi*

Cite This: *ACS Appl. Bio Mater.* 2022, 5, 3563−3572

Read Online

ACCESS | Metrics & More | Article Recommendations

ABSTRACT: Coronavirus disease (COVID-19) is an infectious disease that has posed a global health challenge caused by the SARS-CoV-2 virus. Early management and diagnosis of SARS-CoV-2 are crucial for the timely treatment, traceability, and reduction of viral spread. We have developed a rapid method using a Graphene-based Field-Effect Transistor (Gr-FET) for the ultrasensitive detection of SARS-CoV-2 Spike S1 antigen (S1-Ag). The in-house developed antispike S1 antibody (S1-Ab) was covalently immobilized on the surface of a carboxy functionalized graphene channel using carbodiimide chemistry. Ultraviolet−visible spectroscopy, Fourier-Transform Infrared Spectroscopy, X-ray Photoelectron Spectroscopy (XPS), Atomic Force Microscopy (AFM), Optical Microscopy, Raman Spectroscopy, Scanning Electron Microscopy (SEM), Enzyme-Linked Immunosorbent Assays (ELISA), and device stability studies were conducted to characterize the bioconjugation and fabrication process of Gr-FET. In addition, the electrical response of the device was evaluated by monitoring the change in resistance caused by Ag−Ab interaction in real time. For S1-Ag, our Gr-FET devices were tested in the range of 1 fM to 1 μM with a limit of detection of 10 fM in the standard buffer. The fabricated devices are highly sensitive, specific, and capable of detecting low levels of S1-Ag.

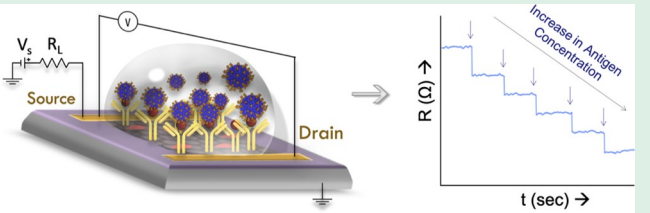

Gr-FET based immunosensing of SARS-CoV-2

KEYWORDS: *SARS-CoV-2, field-effect transistor, graphene, SARS-CoV-2 Spike S1 antigen, MERS-CoV antigen*

1. INTRODUCTION

"Coronavirus disease 2019" (COVID-19) is a human viral infection that causes severe respiratory distress. At the end of 2019, a spate of bronchopneumonia cases with no known etiology were recorded in Wuhan, China.[1] Globally as of 26th May 2022, there have been 529,852,263 cases of COVID-19, causing over 6,306,538 deaths worldwide.[2]

SARS-CoV-2 is a single-stranded positive RNA virus. Spike (S), nucleocapsid (Nuc), envelope (E), and matrix (M) are four important structural proteins of coronavirus.[3,4] Severe acute respiratory syndrome virus (SARS-CoV) and Middle East respiratory syndrome virus (MERS-CoV) have caused major epidemics during the last two decades. The novel virus was named SARS-CoV-2 due to its genomic similarity with SARS-CoV, MERS-CoV, and bat coronavirus RaTG13.[5] According to one phylogenetic analysis, angiotensin-converting enzyme II (ACE2), present in the mammalian cells is used by SARS-CoV-2 to facilitate the viral entry into the cell.[3,6,7]

Currently, chest computed tomography (CT),[8] the real-time reverse-transcriptase polymerase chain reaction (RT-PCR),[9] and the lateral flow-based chromatographic strip[8,10] are considered to be the three main diagnostic techniques. However, both the CT scans and RT-PCR that are available in hospitals take longer time, are costly, and necessitate the use of skilled professionals. Furthermore, a CT scan can only detect the acuteness of a disease but cannot identify the specific virus strain present, based on these symptoms. In addition to that, a CT scan involves the usage of a high dose of radiation, and there is a chance of misinterpretation.[11] Hence, highly sensitive and reliable diagnostic techniques are required for rapid detection of viral antigen.

Advancement in serological assays and biosensors has made them viable alternatives to conventional techniques. Detection methods such as enzyme-linked immunosorbent assays (ELISA),[12−14] electrochemical sensors,[15−18] field-effect transistors (FET),[19] nanosensors,[20,21] and so forth are gaining a lot of attention due to their advantages over traditional methods. Recently, an FTO-based immunosensor was developed for the detection of the receptor-binding domain of SARS-CoV-2 with a limit of detection (LOD) of 0.73 fM.[22] There are various biorecognition elements used to provide analyte specificity in biosensors. Antibodies, enzymes, nucleic acid, aptamers, and molecularly imprinted polymers are some of the biomolecules

Received: May 30, 2022
Accepted: June 23, 2022
Published: July 1, 2022

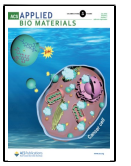

https://doi.org/10.1021/acsabm.2c00503
ACS Appl. Bio Mater. 2022, 5, 3563−3572

Scheme 1. Schematic Illustration of the Gr-FET Fabrication and Biosensing Process, (a) Precleaned Si/SiO_2 Substrate, (b) Graphene Exfoliated on Si/SiO_2 Using the Scotch Tape Method, (c) EBL Was Performed to Define Source (S) and Drain (D) Contacts Accompanied by Metallization with 5/50 nm Cr/Au Respectively, (d) Activation of Graphene Channel Was Performed Using EDC/NHS Carbodiimide to Bind SARS-CoV-2 S1-Ab (Ab), (e) Immobilization of Ab and Blocking of Nonspecific Binding Sites Using BSA, (f) Sensing Was Performed by Addition of Various Concentrations of Ag, Starting From 1 fM to 1 μM to the Ab Functionalized Graphene[a]

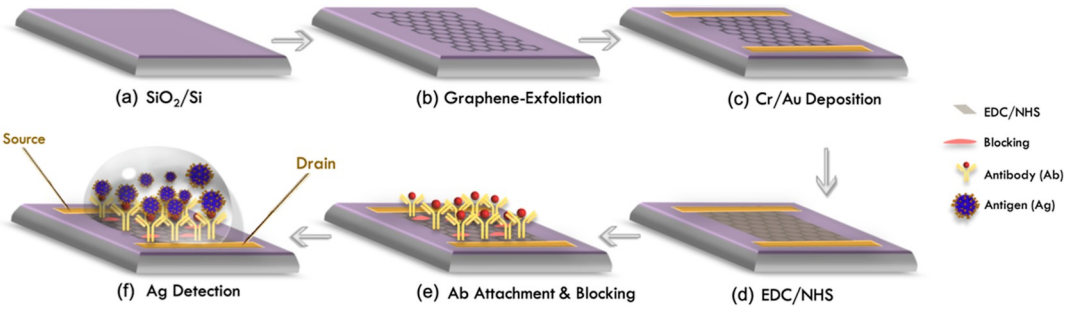

[a]The real-time measurement of resistance (R) as a function of time (t) was recorded at each step to monitor the sensing potential of the device.

used for the detection of target molecules. The advantage of antibodies over other biorecognition elements such as DNA and aptamers are lower cost, high affinity, highly stable, ease of functionalization, immobilization on different sensing elements such as graphene, and their capability to bind to a target, in different physiological conditions of clinical samples.[19,23] In addition to that, several advanced nanomaterials such as gold nanoparticles, iron oxide nanoparticles, organogels,[24] and carbon nanotubes,[25−27] graphene have proven to be superior conductive materials to enhance the sensitivity of biosensors.[28,29] Graphene is a hexagonal two-dimensional (2D) material that has outperformed other nanomaterials in the construction of sensitive biosensors.[29−34] Due to their immense potential, graphene-based FETs are successfully employed for the development of various diagnostic platforms.[35−37]

FET sensors are other electrochemical sensors gaining a lot of attention due to their sensitivity, fast sensing ability, label-free operation, low cost, and miniaturization.[38] They have the potential to offer ultrahigh sensitivity and may be applied to develop portable point-of-care testing devices. The added benefit for FET-based sensors over other label-free electrochemical or capacitance-based sensors is the ultra-low amounts of analyte required for detection.[38,39] Several FET-based sensors have been reported to detect the ultrasensitive detection of SARS-CoV-2. However, most of these sensors are still presenting some challenges such as the complex design of fabrication.

In this study, we used in-house generated Spike S1 antibody (S1-Ab) modified graphene to develop a CoV-sensing FET device for the detection of SARS-CoV-2 Spike S1 antigen (S1-Ag). The major advantage of this FET sensor over other published FET devices is that, here, in-housed generated Spike S1 antibodies were used for the sensing, which reduces the overall cost of sensor fabrication. Furthermore, among top-down lithography, electron beam lithography (EBL) showed the ability to create synthetic surfaces with sub-50 nm spatial resolution and a well-defined control of the topographical features to decorate the electrode with high-resolution nanostructures.[40] Graphene-based FETs were fabricated by the conventional Scotch-tape exfoliation process on SiO_2/Si substrate, followed by standard EBL and metallization with 5/50 nm Cr/Au.[41−43] The S1-Ab were raised in-house[15] and covalently conjugated with graphene, using carbodiimide chemistry.[29,44] Interaction of S1-Ag with graphene-conjugated S1-Ab results in the redistribution of local doping, thus the change in resistance of graphene, which can rapidly be detected as an output as illustrated in Scheme 1. Each step of fabrication, antibody conjugation, and antigen−antibody (S1-Ag/S1-Ab) interaction was ensured with different characterization using Ultraviolet−visible (UV−vis) spectroscopy, Raman Spectroscopy, Atomic Force Microscopy (AFM), Fourier-Transform Infrared Spectroscopy (FT-IR), X-ray Photon Spectroscopy (XPS), Optical Imaging, and Scanning Electron Microscopy (SEM). Our results demonstrate the successful fabrication of Gr-FET devices, which can detect S1-Ag with the LOD of 10 fM that could potentially be used for the development of a portable, miniaturized sensor for the detection of SARS-CoV-2.

2. MATERIALS AND METHODS

2.1. Reagents and Materials. New Zealand white rabbit (6−8 weeks of age) was acquired from Vyas Labs, Hyderabad. SARS-CoV-2 Spike S1 Ag and MERS-CoV were procured from R&D Systems (Minnesota, USA). Micro Chem Corp (Newton, MA, USA) provided poly(methyl methacrylate) (PMMA) 495 and 950. The chemicals for conjugation and immunization, such as 1-ethyl-3-(3-dimethylaminopropyl)carbodiimide hydrochloride (EDC), *N*-hydroxysulfosuccinimide (sulfo-NHS), bovine serum albumin (BSA), Freund's complete adjuvant (FCA), and Freund's incomplete adjuvant (FIA), were procured from Sigma-Aldrich (Delhi, India). Generated antibodies were purified with Protein-A Sepharose resin [Cytiva (Marlborough, USA)]. Tetramethylbenzidine (TMB) was procured from HiMedia (Mumbai, India). Proteintech (Rosemont, Illinois, USA) provided the secondary antibody [goat antirabbit horseradish peroxidase (HRP) labeled Ab]. Chromium pellets and gold wires (99.9%), used for thermal evaporation were provided by Kurt J. Lesker Co. (Clairton, PA, USA), while a single crystal of Kish graphite was procured from Covalent Materials Corp. (Tokyo, Japan). 3M Scotch tape was used to exfoliate graphene. The SiO_2(285 nm)/Si substrates were procured from Nova Electronic Materials (TX, USA).

2.2. Instruments. Bio-Rad Mini-PROTEAN Tetra vertical electrophoresis cell was used to prepare and run the sodium dodecyl-sulfate polyacrylamide gel electrophoresis (SDS-PAGE). Gel images were analyzed in a Thermo Fisher Scientific iBright CL1500 imaging system (Bangalore, India). A Systonic S-924 single beam UV−vis spectrophotometer (Delhi, India) was used to measure the UV−vis spectra, while FT-IR spectra were taken and analyzed on a "Thermo Scientific-Nicolet iS50 FT-IR spectrometer" (Bangalore,

https://doi.org/10.1021/acsabm.2c00503
ACS Appl. Bio Mater. 2022, 5, 3563−3572

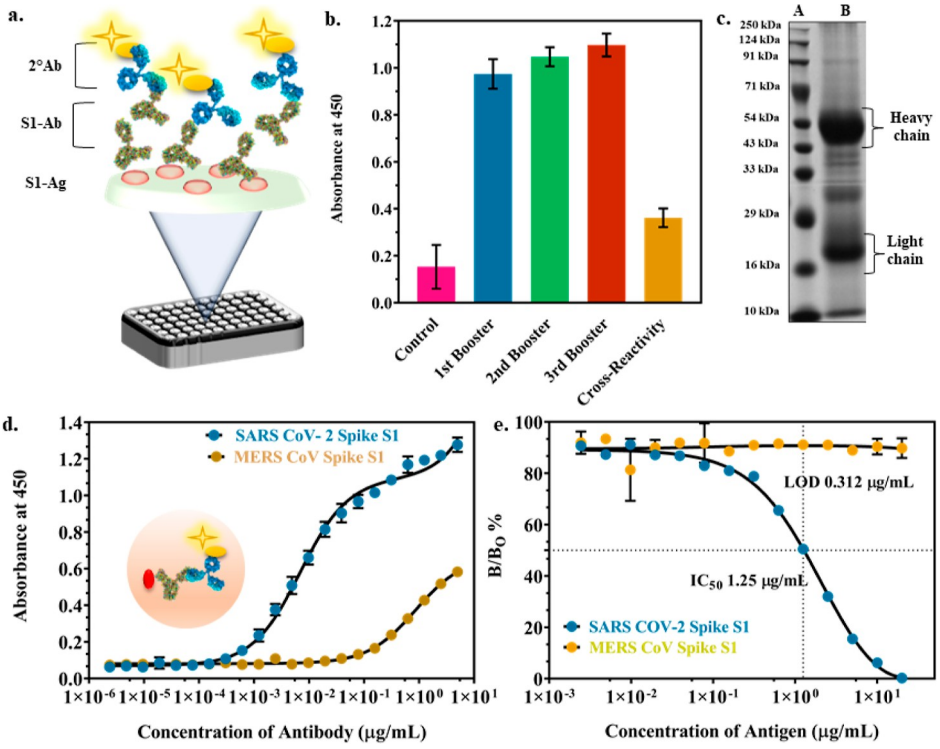

Figure 1. Characterization and immunoassay development for Spike S1 Ab; (a) pictorial representation of indirect-binding ELISA; (b) bar graph representing the serum titer of Ab after each booster, along with preimmune sera and cross-reactivity with MERSCoV; (c) 10% SDS-PAGE of S1-Ab (lane A): depicting protein ladder; (lane B) heavy (50 kDa) and light chain of Ab; (d) binding ELISA of S1-Ab with S1-Ag and MERS-CoV Ag; and (e) competitive ELISA indicating the LOD of 0.312 μg/mL.

India), respectively. XPS (AXIS Supra+, KRATOS Analytical) was used to determine elemental composition. The Renishaw in Via Raman microscope was used to obtain the Raman spectra of graphene (Bangalore, India). Scanning electron microscopes Hitachi S-3400N and Ultra55 Carl Zeiss Mono with an acceleration voltage of 3 kV (Bangalore, India) were used for examining the surface morphology. Optical measurements were taken with an Olympus BX 51 microscope (Bangalore, India). EBL was performed using a Raith e-Lline (Bangalore, India). A PerkinElmer Thermo Fisher Scientific Multiskan FC microplate photometer (Bangalore, India) was used to scan ELISA readings. All the electrical measurements were performed at 227.7 Hz with SRS 830 lock-in amplifier as a carrier frequency. Keithley 2400 source meter was used to apply the gate voltage (V_g). Unless otherwise stated, all experiments were carried out under room temperature (RT) conditions (25 °C).

2.3. Generation, Purification, and Characterization of SARS-CoV-2 S1-Ab. 186 μg of S1-Ag was emulsified with an equal amount of FCA and administered subcutaneously in a New Zealand white rabbit (6−8 weeks of age). Following that, three boosters emulsified with FIA were administered at 15 days intervals. The serum was collected from rabbits after each booster. Protein-A Sepharose was used to purify S1-Ab, and further, phosphate buffer saline (PBS) was used to dialyze the purified fractions together (pH 7.4). Purified S1-Ab was evaluated by running it on 10% SDS-PAGE. Further, to screen the binding of S1-Ab, competitive ELISA was performed. Subsequently, the sensitivity of the immunoassay was compared with the developed CoV-FET sensor.

Indirect binding ELISA was used to standardize the optimum concentration of S1-Ab, to be used for the competitive assay. 96-Well plates were coated with 0.25 μg/mL of S1-Ag and incubated for 16−17 h in a cold room. Unbound Ag was removed from the ELISA plates by washing it 3 times with PBS-T (PBS with 0.02% Tween 20), followed by blocking the plates with 2% PBS-M (PBS with 2% dry milk/skimmed milk) for 1 h at 37 °C. After incubation, plates were given a triple wash to remove the blocking solution, and 100 μL S1-Ab was added per well in duplicates at concentrations varying from 5 to 2.38 × 10^{-6} μg/mL diluted in PBS-M (0.1%) for 2 h. Post incubation, HRP-conjugated secondary Ab (1:10,000 dilution in 0.1% PBS-M) was added and incubated for 1 h at 37 °C. Each well received a total of 100 μL of TMB substrate, the plates were incubated for 15 min in dark to avoid false color development. The reaction was stopped by the addition of 1 N H_2SO_4 and readings were taken at 450 nm. The cross-reactivity was also evaluated with the same procedure for MERSCoV Spike S1 Ag.

Optimized parameters and concentration obtained from the binding ELISA were used to perform competitive ELISA. All the initial steps were the same, as previously performed for the binding ELISA. However, after blocking, S1-Ag was serially diluted in the range from 10 to 3.05 × 10^{-4} and incubated with a fixed concentration of S1-Ab (0.3125 μg/mL) and added to the 96-well plate. All the remaining steps were the same. Similarly, the cross-reactivity of the immunoassay was analyzed with serially diluted MERS-CoV Ag (10−3.05 × 10^{-4}) with S1-Ab (0.3125 μg/mL).

2.4. Bioconjugation and Characterization of S1-Ab Modified Graphene (Graphene/Ab). Graphene/Ab conjugate was prepared by EDC/NHS-based carbodiimide chemistry. Briefly, 75 mM of each EDC and NHS was added to 1 mg graphene to activate the carboxyl group. The solution was gently stirred for 2.5 h at RT, centrifuged (10,000 rpm at 4 °C), and washed with PB (50 mM, pH 7.4) to discard any unreacted coupling reagent. The activated graphene was dispersed in the PB buffer, and S1-Ab was added dropwise. The graphene/Ab complex was incubated for 30 min at RT and later, incubated overnight (O/N) at 4 °C.[44] The remaining active site of graphene was blocked with 2% BSA in 50 mM PB. The solution was again centrifuged to remove any unbound molecules, and graphene/Ab complex was treated with S1-Ag for 2 h at RT. Each step of aconjugation was characterized using UV−vis spectroscopy, FT-IR (400−4000 cm^{-1}), SEM, XPS and AFM.

2.5. Fabrication of the Gr-FET Device. For the fabrication of graphene-based FETs, graphene was exfoliated from a single crystal of graphite on a precleaned (acetone−IPA and RCA cleaned) 285 nm SiO_2/Si substrate using the traditional Scotch tape method, using

https://doi.org/10.1021/acsabm.2c00503
ACS Appl. Bio Mater. 2022, 5, 3563−3572

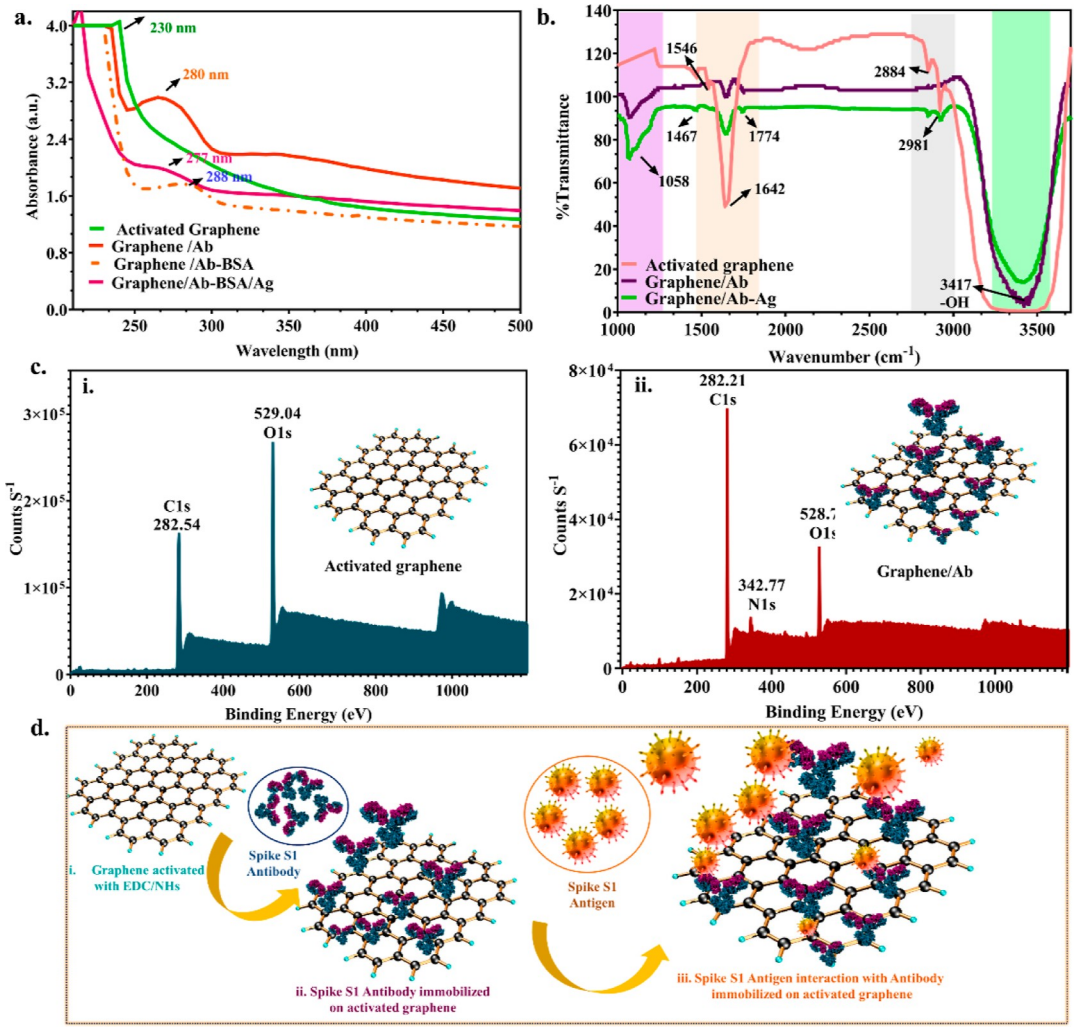

Figure 2. Characterization of activated graphene and graphene/Ab (a) UV−vis spectra depicting the different peaks of graphene, graphene/Ab, and graphene/Ab−Ag; (b) FT-IR spectra of activated graphene, graphene/Ab, and graphene/Ab−Ag; (c) XPS survey scan (i) C 1s and O 1s spectra of activated graphene (ii) C 1s, O 1s, and N 1s spectra of graphene/Ab; (d) different steps of graphene activation, antibody immobilization, and interaction of antigen with graphene immobilized antibody.

SiO_2 as the back-gate dielectric. After exfoliation, monolayer graphene was tracked down using a high-resolution optical microscope from 200 to 1000 magnification. PMMA 495 and PMMA 950 (positive resist) were spin-coated on the graphene exfoliated substrates and baked at 150 °C to define electrode patterns using EBL. Later, samples were developed in a 3:1 solution of isopropanol and methyl isobutyl ketone followed by rinsing in IPA. The Cr/Au electrodes of thickness 5 and 50 nm, respectively were deposited using a thermal evaporation system under ultra-high vacuum conditions, and the samples were kept overnight in acetone for the lift-off process. Finally, the substrates were mounted on a ceramic chip carrier with silver epoxy, and electrodes were ball-bonded with an Au wire bonder machine.[44−47]

2.6. Electrochemical Analysis of Graphene/Ab on the Fabricated Gr-FET Device. The S1-Ab was immobilized on the activated surface of the graphene channel. The PB buffer was used as a washing solvent at every step to wash any excess or unbound material. The device was employed for analyte detection after blocking. Different concentrations of S1-Ag (1 fM to 1 μM) were prepared for electrochemical sensing as detailed in Scheme 1. Liquid state measurements were taken, and change in resistance was measured at every stage using a constant current circuit that allows 100 nA of current via a graphene channel. The repeatability of Gr-FET was tested using three devices by the addition of known concentrations of Ag and monitoring the channel resistance in real time. In addition, the specificity of the proposed device was tested for cross-reactivity with MERS-CoV Ag.

3. RESULTS AND DISCUSSION

3.1. Fabrication and Characterization of the Biosensing Device. Scheme 1 depicts the various stages involved in the fabrication of Gr-FET. As explained before, the Scotch tape method was used to exfoliate graphene on a precleaned SiO_2/Si substrate (Scheme 1a,b). EBL and thermal evaporation were performed to define the source (S) and drain (D) contacts (Scheme 1c). After mounting the graphene device on the chip carrier, the channel was functionalized or activated with EDC/NHS carbodiimide chemistry (detailed before) to immobilize S1-Ab onto it. Blocking of any remaining nonspecific binding sites was performed using BSA (Scheme 1e) to ensure the specificity of the device. Finally, graphene-based biosensing experiments were executed by continuous monitoring of the change in resistance at every step (Scheme 1f).

3.2. Characterization and Validation of In-House Generated S1-Ab. Generated in-house antibody was characterized and validated by the indirect binding ELISA, SDS-PAGE, and detection limit was determined by the

https://doi.org/10.1021/acsabm.2c00503
ACS Appl. Bio Mater. 2022, 5, 3563−3572

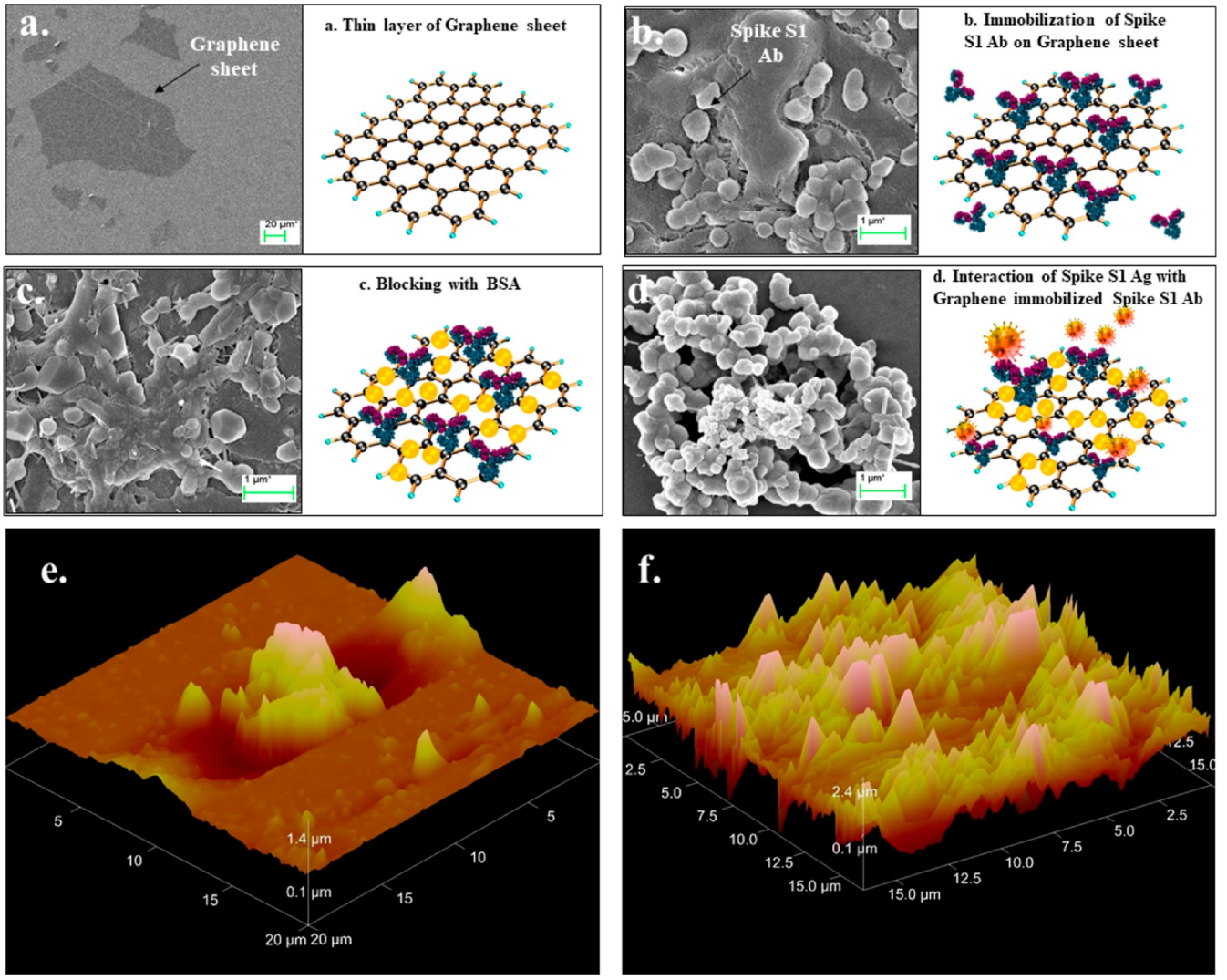

Figure 3. Microscopic characterization of graphene, graphene/S1-Ab, and graphene/S1-Ab−Ag; (a) SEM images indicating the thin layer of a graphene sheet on the Si/SiO_2 substrate; (b) deposition of antibody on the graphene; (c) BSA blocking; (d) antigen−antibody complex; (e,f) AFM image of graphene and S1-Ab immobilized on the graphene sheet.

competitive ELISA. Figure 1a depicts the 2-step indirect binding ELISA, where primary antibody was incubated with the antigen, followed by the enzyme linked secondary antibody to determine the titer of antibody. The serum after each booster was collected, and the Ab titer was measured with indirect binding ELISA Figure 1. Titer was increased after each booster, while negligible binding was detected in preimmune sera (control) along with slight binding with MERS-CoV Ag (due to its close similarity with SARS-CoV-2) as shown in Figure 1b. After purification of serum, 10% SDS PAGE was performed, which revealed fragment bands at 50 and 25 kDa for the heavy and light chains of S1-Ab (IgG) (Figure 1c), respectively. According to binding ELISA, the optimum concentration for competitive ELISA was 0.25 μg/mL of S1-Ag and 0.31 μg/mL of S1-Ab (Figure 1d). In addition to binding ELISA, the specificity of S1-Ab was evaluated with MERS-CoV Ag. Negligible cross-reactivity was observed. The competitive ELISA of S1-Ag and S1-Ab showed a detection limit of 0.312 μg/mL (Figure 1e). The in-housed generated S1-Ab has a higher affinity for SARS-CoV-2 Ag in comparison to MERS-CoV Ag in both the binding and competitive ELISA. Thus, it has been concluded that S1-Ag and S1-Ab have the potential to be used for the development of electrochemical sensors with negligible cross reactivity.

3.3. Characterization of Graphene and S1-Ab Labeling. Recently, graphene emerged as a catalytic coating material for the electrode due to its superior electrical conductivity and mobility. Activation of graphene and antibody bioconjugation was confirmed with UV−vis spectroscopy, FT-IR, and XPS. As shown in Figure 2a activated graphene displayed the typical absorbance peak at 230 nm. After S1-Ab bioconjugation on the surface of graphene, the resultant showed two absorption peaks at 230 and 280 nm, in which 280 nm corresponds to the antibody peak. Additionally, BSA and Ag incorporation led to a red shift of 8 nm (280−288 nm). Figure 2b shows the FT-IR spectra of activated graphene, graphene/Ab, and graphene/Ab−Ag. FT-IR spectra provide evidence for the presence of oxygen-containing functional groups in all the samples. A fairly broad peak in the region around 3700 to 3000 cm^{-1} is due to the stretching vibration of the hydroxyl group (C−OH), which is a characteristic peak of activated graphene. The two small peaks near ∼2981 and ∼2884 cm^{-1} can be observed in activated graphene corresponding to the hydrogen-bonded −OH group of the dimeric −COOH group, and intra-

https://doi.org/10.1021/acsabm.2c00503
ACS Appl. Bio Mater. 2022, 5, 3563−3572

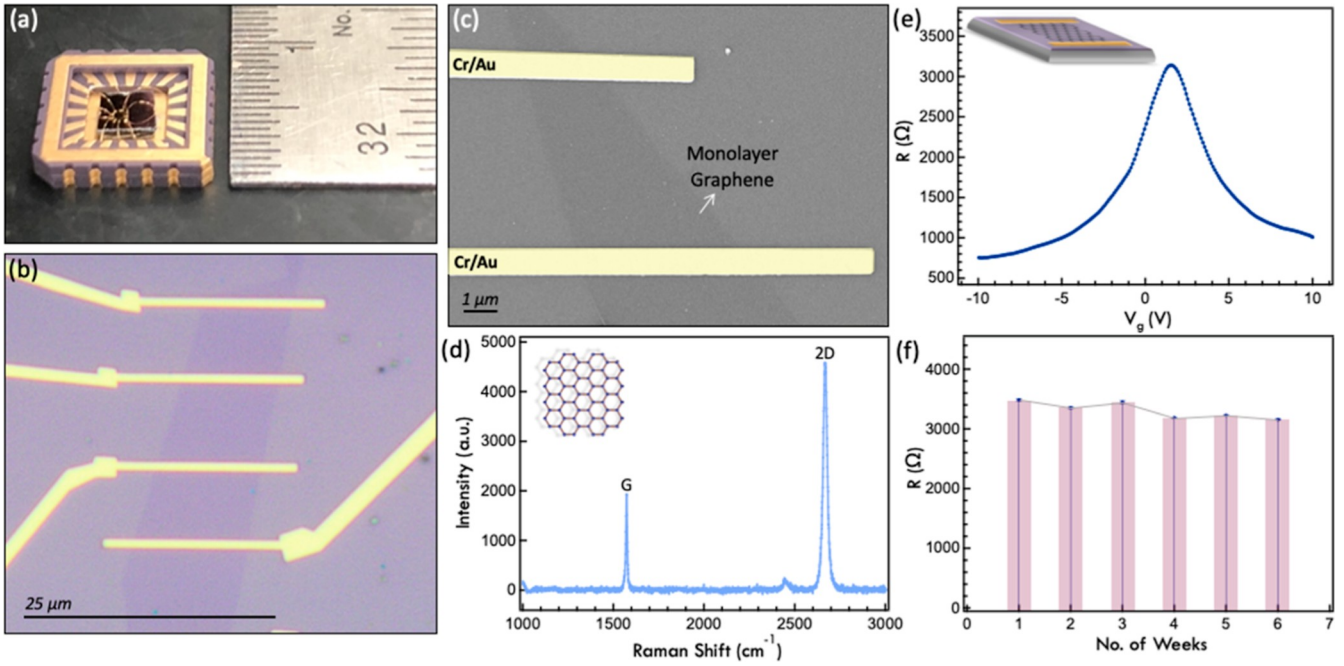

Figure 4. (a) Picture of the wire-bonded Gr-FET device on a ceramic chip carrier, the scale unit is in cm, (b) optical image of the pristine Gr-FET device, (c) SEM image of the Gr-FET device top contacted with Cr/Au electrodes, the false yellow coloring is used for enhancing visual illustration, (d) Raman spectra of monolayer graphene showing typical characteristics of G and 2D peaks (e) resistance (R) as a function of gate voltage (V_g) plot of Gr-FET, (f) stability plot obtained by measuring R vs t over a span of 6 weeks.

molecular bonded −OH stretching of alcohols. The peak in the low frequency, close to ∼1642, is due to O−H vibrations. The emergence of the peak at ∼1058 cm^{-1}, related to characteristic C−N stretching of amide due to the presence of S1-Ab conjugated with graphene via carbodiimide chemistry, confirms the binding of antibodies onto the graphene. The chemical composition of graphene and graphene/Ab was determined by XPS. In the survey spectra of both graphene and graphene/Ab, photoelectron lines for C 1s and O 1s confirm the presence of C and O.[48,49] Graphene/Ab has an additional line for N 1s, which further confirms the presence of nitrogen of antibody bound with graphene Figure 2c(i,ii). Different steps of bioconjugation of graphene with S1-Ab and interaction of the Ab−Ag complex are depicted in Figure 2d.

SEM image of graphene and activated graphene with S1-Ab is depicted in Figure 3, which shows a thin layer of graphene in Figure 3a. Further, morphological characteristics of different steps of bioconjugation were also observed in SEM. Antibody immobilized on graphene was confirmed by the presence of a globular structure on the surface of graphene (Figure 3b), BSA blocking (Figure 3c), and the Ag−Ab complex on graphene (Figure 3d). Topographic images of graphene and graphene/Ab are shown in Figure 3e,f, together with the height profile. Graphene has a lateral dimension of 839 nm. Furthermore, we can clearly see a change in the height after the addition of the antibody, which confirmed the formation of the graphene/Ab complex.

3.4. Characterization of the Gr-FET Biosensing Device. Figure 4a shows the picture of the packaged Gr-FET device Au-wire bonded to a ceramic chip carrier. The optical and SEM image of typical monolayer graphene on SiO_2/Si wafer after EBL and the metallization step is shown in Figure 4b,c, respectively. Raman spectroscopy was performed to confirm the monolayer graphene and its quality. The typical Raman characteristic of G and 2D peaks at ∼1580 and 2670 cm^{-1}, respectively, was observed with an I_{2D}/I_G ratio >2, which confirms the presence of single-layer graphene.[50] Moreover, the absence of the D peak which typically appears at ∼1350 cm^{-1} exhibit the formation of high-quality monolayer graphene with negligible defects (Figure 4d). The resistance (R) as a function of gate voltage (V_g) measurement was conducted in constant the current (CC) mode, where V_g was swept from 10 to −10 V, as depicted in Figure 4e. The bell shape curve across a wide range of V_g demonstrates the ambipolar behavior of the graphene channel with a charge neutrality point or the Dirac point at ∼1.5 V. The electrical performance of Gr-based devices is sensitive to polar molecules present in the environment. The change in environmental conditions such as highly humid conditions can significantly affect the stability of Gr-FET devices. This can cause uncertainty in evaluating the doping level of graphene and the subsequent amount of detected molecules.[51,52] To test the stability of Gr-FET devices, we monitored the channel resistance of our samples every week (in air) under ambient lab conditions (humidity < 30%). As shown in Figure 4f, a very small change in resistance was observed over a period of 6 weeks which demonstrates the stability of our devices. In order to ensure there is no response from the gold electrode, we checked the response of Ab−Ag standard Au-FET, the negligible response confirms that Au electrodes do not contribute toward any change in resistance.[53]

3.5. Detection of S1-Ag Using the Gr-FET Sensor in Real Time. To investigate the potential of the Gr-FET sensor for the detection of SARS-CoV-2 Ag, we evaluated the kinetic response at every step for various devices. The real-time change in resistance was measured in the CC mode at zero bias V_g and a constant current of 100 nA. As shown in Figure 5a, the Gr-FET channel was initially rinsed with PB solution in order to account for any resistance changes that may happen on PB addition as all the aliquots are made in PB. The change in resistance on PB addition possibly suggests diffusion of ions

https://doi.org/10.1021/acsabm.2c00503
ACS Appl. Bio Mater. 2022, 5, 3563−3572

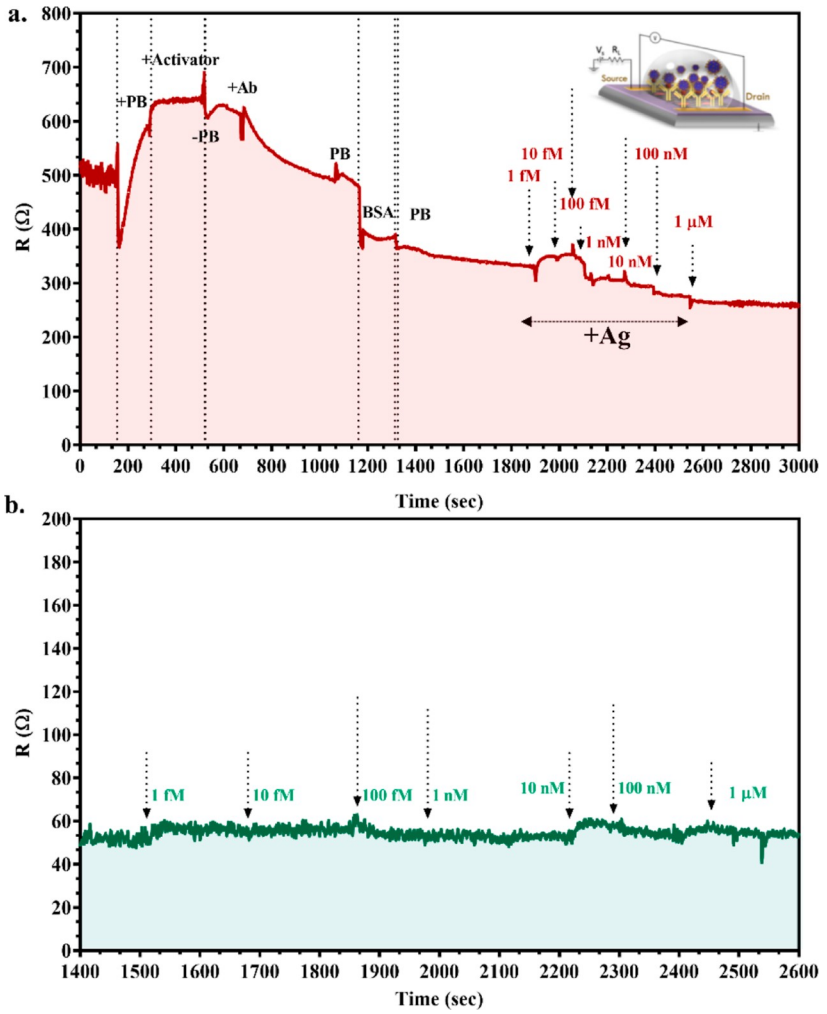

Figure 5. The kinetic response of the Gr-FET device functionalized with S1-Ab at various concentrations of (a) SARS-CoV-2 Ag added, ranging from 1 fM to 1 μM in 50 mM PB (pH 7.2) and (b) MERS-CoV Ag of various concentrations added (1 fM to 1 μM) in PB.

from PB into the graphene channel. On activation with EDC/NHS to immobilize the Ab, enhancement in resistance was observed, which could be assigned to the p doping of the graphene channel by the carboxylic group.[54] The channel was then treated with S1-Ab solution, where a drop in resistance indicates the surface charge de-doping effect due to the interaction between ionic species or the coupling effects of the activator and Ab on the graphene channel. After some time, PB rinsing was performed to eliminate any excess unbound Ab on the surface of the channel. BSA treatment was carried out to block the remaining free nonspecific binding sites, followed by PB rinsing to intensify and ensure the interaction of Ag to the immobilized Ab alone and not to the free sites of graphene that may eventually contribute toward a change in the channel *R*. On subsequent addition of SARS-CoV-2 Ag from 1 fM to 1 μM, a clear change in *R* was noticed due to the heterogeneous electron transfer between Ab−Ag interaction.[53] A gradual drop in *R* was observed with an increase in Ag concentration which saturates after 1 μM. This effect has already been reported in FETs, which can be attributed to the change in doping level due to the interaction of Ag−Ab at the reactive site on graphene and the solution interface that essentially changes the overall electrostatic potential (Δq) of the channel, which causes the Dirac point to shift ($\Delta V_{\text{Dirac}} = \Delta q/C$), where *C* is the gate capacitance of Gr-FET.[18,44] It is important to note that the large surface area of graphene leads to more efficient sensing by providing a greater number of active sites for Ag−Ab interaction. For quantitative analysis of device response, the sensitivity of the device was evaluated by calculating the change in channel resistance (ΔR) (in %) by selecting R_{PB} as the baseline. The ΔR (%) of ∼5.4 to 20.6% was obtained for SARS-CoV-2 Ag concentrations ranging from 1 fM to 1 μM. However, no significant signal, that is change in *R*, was observed upon the addition of MERS-CoV.

Ag, as depicted in Figure 5b, indicates the specificity and sensitivity of our S1-Ab functionalized Gr-FET to Spike S1 Ag. Moreover, negligible change in *R* on MERS-CoV Ag addition can be ascribed to the efficient Ab binding to the channel and blocking of nonspecific sites achieved by BSA.

4. CONCLUSIONS

From this study, it is concluded that we have developed a Gr-FET sensor, where SARS-CoV-2 S1-Ab was immobilized on the surface of graphene and can be used as a sensing element. The binding of Ag with graphene-labeled Ab resulted in the redistribution of local doping and change in the graphene conductivity. The developed sensor was able to read the change in resistance and further analyze the proportion of antigen with a detection limit of 10 fM. Furthermore, the devices have shown negligible cross-reactivity with MERS-

https://doi.org/10.1021/acsabm.2c00503
ACS Appl. Bio Mater. 2022, 5, 3563−3572

CoV, which overall increases the specificity of the developed sensor. Thus, this sensor could be used as an alternative, cost-effective device for the detection of SARS-CoV-2. Additionally, this developed Gr-FET sensor could potentially be miniaturized to develop a portable sensing platform for the diagnosis of SARS-CoV-2 and can be adapted for personalized healthcare in the near future.

AUTHOR INFORMATION

Corresponding Authors

Arindam Ghosh − *Department of Physics and Centre for Nano Science and Engineering (CeNSE), Indian Institute of Science (IISc), Bangalore 560012, India*; Phone: +91 80 2293 3288; Email: arindam@iisc.ac.in

Sonu Gandhi − *DBT-National Institute of Animal Biotechnology (DBT-NIAB), Hyderabad 500032 Telangana, India*; orcid.org/0000-0003-0960-2780; Phone: +91 40 23120127; Email: gandhi@niab.org.in

Authors

Deepshikha Shahdeo − *DBT-National Institute of Animal Biotechnology (DBT-NIAB), Hyderabad 500032 Telangana, India*

Neha Chauhan − *Department of Physics, Indian Institute of Science (IISc), Bangalore 560012, India; The Solid State and Structural Chemistry Unit, Indian Institute of Science, Bangalore 560012, India*

Aniket Majumdar − *Department of Physics, Indian Institute of Science (IISc), Bangalore 560012, India*

Complete contact information is available at: https://pubs.acs.org/10.1021/acsabm.2c00503

Author Contributions

⊥D.S. and N.C. contributed equally to this paper.

Notes

The authors declare no competing financial interest.

Ethics Approval: All animal experimentations were conducted at Small Animal Facility, National Institute of Animal Biotechnology (NIAB), Hyderabad after due approval from the Institutional Animal Ethics Committee (IAEC-IAEC/2020/NIAB/04/SG). All the cloning and biosafety work was conducted at NIAB after due approval of the Institutional Biosafety Committee (IBSC) with the approval number # IBSC/May2020/NIAB/SG-01.

ACKNOWLEDGMENTS

The authors would like to thank Dr. Jayant Hole for providing support with animal experimentation. S.G. is grateful for the research endowment under the Intensification of Research in High Priority Area (IRHPA) program from the Science and Engineering Research Board (SERB), New Delhi (grant number IPA/2020/000069). N.C. would like to acknowledge the Raman Post-Doc Program, an initiative by the Institution of Eminence (IoE) by the Government of India, at the Indian Institute of Science, Bangalore. She would also like to thank Aparna Parappurath for bonding graphene-FET devices. We thank National Nanofabrication Centre (NNFC) and Micro and Nano Characterization Facility (MNCF) at the Centre for Nano Science and Engineering (CeNSE), IISc, Bangalore, funded by MCIT and DST, Government of India for fabrication and characterization facilities.

REFERENCES

(1) Seo, G.; Lee, G.; Kim, M. J.; Baek, S.-H.; Choi, M.; Ku, K. B.; Lee, C.-S.; Jun, S.; Park, D.; Kim, H. G.; Kim, S.-J.; Lee, J.-O.; Kim, B. T.; Park, E. C.; Kim, S. I. Rapid Detection of COVID-19 Causative Virus (SARS-CoV-2) in Human Nasopharyngeal Swab Specimens Using Field-Effect Transistor-Based Biosensor. *ACS Nano* **2020**, *14*, 5135−5142.

(2) COVID Live—Coronavirus Statistics—Worldometer. https://www.worldometers.info/coronavirus/ (accessed April 30, 2022).

(3) Roberts, A.; Chouhan, R. S.; Shahdeo, D.; Shrikrishna, N. S.; Kesarwani, V.; Horvat, M.; Gandhi, S. A Recent Update on Advanced Molecular Diagnostic Techniques for COVID-19 Pandemic: An Overview. *Front. Immunol.* **2021**, *12*, 732756.

(4) Mahmud, N.; Anik, M. I.; Hossain, M. K.; Khan, M. I.; Uddin, S.; Ashrafuzzaman, M.; Rahaman, M. M. Advances in Nanomaterial-Based Platforms to Combat COVID-19: Diagnostics, Preventions, Therapeutics, and Vaccine Developments. *ACS Appl. Bio Mater.* **2022**, *5*, 2431−2460.

(5) Ding, X.; Yin, K.; Li, Z.; Lalla, R. V.; Ballesteros, E.; Sfeir, M. M.; Liu, C. Ultrasensitive and Visual Detection of SARS-CoV-2 Using All-in-One Dual CRISPR-Cas12a Assay. *Nat. Commun.* **2020**, *11*, 4711.

(6) Kaushik, A. K.; Dhau, J. S.; Gohel, H.; Mishra, Y. K.; Kateb, B.; Kim, N.-Y.; Goswami, D. Y. Electrochemical SARS-CoV-2 Sensing at Point-of-Care and Artificial Intelligence for Intelligent COVID-19 Management. *ACS Appl. Bio Mater.* **2020**, *3*, 7306−7325.

(7) Shetti, N. P.; Mishra, A.; Bukkitgar, S. D.; Basu, S.; Narang, J.; Raghava Reddy, K.; Aminabhavi, T. M. Conventional and Nano-technology-Based Sensing Methods for SARS Coronavirus (2019-NCoV). *ACS Appl. Bio Mater.* **2021**, *4*, 1178−1190.

(8) Cui, F.; Zhou, H. S. Diagnostic Methods and Potential Portable Biosensors for Coronavirus Disease 2019. *Biosens. Bioelectron.* **2020**, *165*, 112349.

(9) Torres, M. D. T.; de Araujo, W. R.; de Lima, L. F.; Ferreira, A. L.; de la Fuente-Nunez, C. Low-Cost Biosensor for Rapid Detection of SARS-CoV-2 at the Point of Care. *Matter* **2021**, *4*, 2403.

(10) Zhu, N.; Zhang, D.; Wang, W.; Li, X.; Yang, B.; Song, J.; Zhao, X.; Huang, B.; Shi, W.; Lu, R.; Niu, P.; Zhan, F.; Ma, X.; Wang, D.; Xu, W.; Wu, G.; Gao, G. F.; Tan, W. A Novel Coronavirus from Patients with Pneumonia in China, 2019. *N. Engl. J. Med.* **2020**, *382*, 727−733.

(11) Fred, H. L. Drawbacks and Limitations of Computed Tomography: Views from a Medical Educator. *Tex. Heart Inst. J.* **2004**, *31*, 345.

(12) Singh, S.; Mishra, P.; Banga, I.; Parmar, A. S.; Tripathi, P. P.; Gandhi, S. Chemiluminescence based immunoassay for the detection of heroin and its metabolites. *Bioimpacts* **2018**, *8*, 53−58.

(13) Xiang, J.; Yan, M.; Li, H.; Liu, T.; Lin, C.; Huang, S.; Shen, C. Evaluation of Enzyme-Linked Immunoassay and Colloidal Gold-Immunochromatographic Assay Kit for Detection of Novel Coronavirus (SARS-Cov-2) Causing an Outbreak of Pneumonia (COVID-19). *medRxiv* **2020**, 2020.02.27.20028787.

(14) Pu, J.; Gao, Y.; Cao, Q.; Fu, G.; Chen, X.; Pan, Z.; Guan, C. Vanadium Metal-Organic Framework-Derived Multifunctional Fibers for Asymmetric Supercapacitor, Piezoresistive Sensor, and Electrochemical Water Splitting. *SmartMat* **2022**, 1−11.

(15) Roberts, A.; Mahari, S.; Shahdeo, D.; Gandhi, S. Label-Free Detection of SARS-CoV-2 Spike S1 Antigen Triggered by Electroactive Gold Nanoparticles on Antibody Coated Fluorine-Doped Tin Oxide (FTO) Electrode. *Anal. Chim. Acta* **2021**, *1188*, 339207.

(16) Roberts, A.; Tripathi, P. P.; Gandhi, S. Graphene Nanosheets as an Electric Mediator for Ultrafast Sensing of Urokinase Plasminogen Activator Receptor-A Biomarker of Cancer. *Biosens. Bioelectron.* **2019**, *141*, 111398.

(17) Mahari, S.; Gandhi, S. Electrochemical Immunosensor for Detection of Avian Salmonellosis Based on Electroactive Reduced Graphene Oxide (RGO) Modified Electrode. *Bioelectrochemistry* **2022**, *144*, 108036.

(18) Shukla, S.; Haldorai, Y.; Khan, I.; Kang, S.-M.; Kwak, C. H.; Gandhi, S.; Bajpai, V. K.; Huh, Y. S.; Han, Y.-K. Bioreceptor-free,

sensitive and rapid electrochemical detection of patulin fungal toxin, using a reduced graphene oxide@SnO2 nanocomposite. *Mater. Sci. Eng., C* **2020**, *113*, 110916.
(19) Cheng, S.; Hideshima, S.; Kuroiwa, S.; Nakanishi, T.; Osaka, T. Label-Free Detection of Tumor Markers Using Field Effect Transistor (FET)-Based Biosensors for Lung Cancer Diagnosis. *Sens. Actuators, B* **2015**, *212*, 329−334.
(20) Deng, J.; Zhao, S.; Liu, Y.; Liu, C.; Sun, J. Nanosensors for Diagnosis of Infectious Diseases. *ACS Appl. Bio Mater.* **2021**, *4*, 3863−3879.
(21) Luo, Y.; Wu, D.; Li, Z.; Li, X.-Y.; Wu, Y.; Feng, S.-P.; Menon, C.; Chen, H.; Chu, P. K. Plasma Functionalized MoSe2 for Efficient Nonenzymatic Sensing of Hydrogen Peroxide in Ultra-Wide PH Range. *SmartMat* **2022**, 1−12.
(22) Shahdeo, D.; Roberts, A.; Archana, G. J.; Shrikrishna, N. S.; Mahari, S.; Nagamani, K.; Gandhi, S. Label Free Detection of SARS CoV-2 Receptor Binding Domain (RBD) Protein by Fabrication of Gold Nanorods Deposited on Electrochemical Immunosensor (GDEI). *Biosens. Bioelectron.* **2022**, *212*, 114406.
(23) Peltomaa, R.; Glahn-Martínez, B.; Benito-Peña, E.; Moreno-Bondi, M. Optical Biosensors for Label-Free Detection of Small Molecules. *Sensors* **2018**, *18*, 4126.
(24) Zhang, Z.; Yu, Y.; Yu, H.; Feng, Y.; Feng, W. Water-Resistant Conductive Organogels with Sensation and Actuation Functions for Artificial Neuro-Sensory Muscular Systems. *SmartMat* **2022**, 1−12.
(25) Pang, J.; Bachmatiuk, A.; Yang, F.; Liu, H.; Zhou, W.; Rümmeli, M. H.; Cuniberti, G. Applications of Carbon Nanotubes in the Internet of Things Era. *Nano-Micro Lett.* **2021**, *13*, 191.
(26) Zhou, K.; Dai, K.; Liu, C.; Shen, C. Flexible Conductive Polymer Composites for Smart Wearable Strain Sensors. *SmartMat* **2020**, *1*, No. e1010.
(27) Zhang, S.; Pang, J.; Li, Y.; Yang, F.; Gemming, T.; Wang, K.; Wang, X.; Peng, S.; Liu, X.; Chang, B.; Liu, H.; Zhou, W.; Cuniberti, G.; Rümmeli, M. H. Emerging Internet of Things Driven Carbon Nanotubes-Based Devices. *Nano Res.* **2022**, *15*, 4613−4637.
(28) Mohammadniaei, M.; Nguyen, H. V.; Tieu, M. V.; Lee, M. H. 2D Materials in Development of Electrochemical Point-of-Care Cancer Screening Devices. *Micromachines* **2019**, *10*, 662.
(29) Shahdeo, D.; Roberts, A.; Abbineni, N.; Gandhi, S. Graphene Based Sensors. *Compr. Anal. Chem.* **2020**, *91*, 175−199.
(30) Justino, C. I. L.; Gomes, A. R.; Freitas, A. C.; Duarte, A. C.; Rocha-Santos, T. A. P. Graphene Based Sensors and Biosensors. *TrAC, Trends Anal. Chem.* **2017**, *91*, 53−66.
(31) Sengupta, J.; Hussain, C. M. Graphene-Based Field-Effect Transistor Biosensors for the Rapid Detection and Analysis of Viruses: A Perspective in View of COVID-19. *Carbon Trends* **2021**, *2*, 100011.
(32) Narlawar, S. S.; Gandhi, S. Fabrication of Graphene Nanoplatelets Embedded "Partition Cartridge" for Efficient Separation of Target-Bound SsDNA during SELEX. *Mater. Today Adv.* **2021**, *12*, 100174.
(33) Han, Q.; Pang, J.; Li, Y.; Sun, B.; Ibarlucea, B.; Liu, X.; Gemming, T.; Cheng, Q.; Zhang, S.; Liu, H.; Wang, J.; Zhou, W.; Cuniberti, G.; Rümmeli, M. H. Graphene Biodevices for Early Disease Diagnosis Based on Biomarker Detection. *ACS Sens.* **2021**, *6*, 3841−3881.
(34) Wang, Y.; Pang, J.; Cheng, Q.; Han, L.; Li, Y.; Meng, X.; Ibarlucea, B.; Zhao, H.; Yang, F.; Liu, H.; Liu, H.; Zhou, W.; Wang, X.; Rummeli, M. H.; Zhang, Y.; Cuniberti, G. Applications of 2D-Layered Palladium Diselenide and Its van Der Waals Heterostructures in Electronics and Optoelectronics. *Nano-Micro Lett.* **2021**, *13*, 143.
(35) Lu, H.-W.; Kane, A. A.; Parkinson, J.; Gao, Y.; Hajian, R.; Heltzen, M.; Goldsmith, B.; Aran, K. The Promise of Graphene-Based Transistors for Democratizing Multiomics Studies. *Biosens. Bioelectron.* **2022**, *195*, 113605.
(36) Yupapin, P.; Mahesha, C. R.; Fouladi, H.; Hamidi, A.; Farmani, A. Recent Advances in CNT-Based FET Transistor Biosensors to Detect Biomarkers of Clinical Significance. *Silicon* **2022**, 1−7.
(37) Alhazmi, H. A.; Ahsan, W.; Mangla, B.; Javed, S.; Hassan, M. Z.; Asmari, M.; Al Bratty, M.; Najmi, A. Graphene-Based Biosensors for Disease Theranostics: Development, Applications, and Recent Advancements. *Nanotechnol. Rev.* **2021**, *11*, 96−116.
(38) Lowe, B. M.; Sun, K.; Zeimpekis, I.; Skylaris, C.-K.; Green, N. G. Field-Effect Sensors—from PH Sensing to Biosensing: Sensitivity Enhancement Using Streptavidin−Biotin as a Model System. *Analyst* **2017**, *142*, 4173−4200.
(39) Bergveld, P.; Wiersma, J.; Meertens, H. Extracellular Potential Recordings by Means of a Field Effect Transistor Without Gate Metal, Called OSFET. *IEEE Trans. Biomed. Eng.* **1976**, *BME-23*, 136−144.
(40) Zanut, A.; Cian, A.; Cefarin, N.; Pozzato, A.; Tormen, M. Nanoelectrode Arrays Fabricated by Thermal Nanoimprint Lithography for Biosensing Application. *Biosensors* **2020**, *10*, 90.
(41) Pal, A. N.; Ghatak, S.; Kochat, V.; Sneha, E. S.; Sampathkumar, A.; Raghavan, S.; Ghosh, A. Microscopic Mechanism of 1/f Noise in Graphene: Role of Energy Band Dispersion. *ACS Nano* **2011**, *5*, 2075−2081.
(42) Karnatak, P.; Sai, T. P.; Goswami, S.; Ghatak, S.; Kaushal, S.; Ghosh, A. Current Crowding Mediated Large Contact Noise in Graphene Field-Effect Transistors. *Nat. Commun.* **2016**, *7*, 13703.
(43) Islam, S.; Shukla, S.; Bajpai, V. K.; Han, Y.-K.; Huh, Y. S.; Kumar, A.; Ghosh, A.; Gandhi, S. A Smart Nanosensor for the Detection of Human Immunodeficiency Virus and Associated Cardiovascular and Arthritis Diseases Using Functionalized Graphene-Based Transistors. *Biosens. Bioelectron.* **2019**, *126*, 792−799.
(44) Roberts, A.; Chauhan, N.; Islam, S.; Mahari, S.; Ghawri, B.; Gandham, R. K.; Majumdar, S. S.; Ghosh, A.; Gandhi, S. Graphene Functionalized Field-Effect Transistors for Ultrasensitive Detection of Japanese Encephalitis and Avian Influenza Virus. *Sci. Rep.* **2020**, *10*, 14546.
(45) Dwivedi, P.; Chauhan, N.; Dhyani, V.; Kumar, D. S.; Dhanekar, S. Design, Fabrication, Characterization and Packaging of Bottom Gate and Nano-Porous TiO2 Based FET. *2017 IEEE 17th International Conference on Nanotechnology, NANO*, 2017; pp 946−950.
(46) Chauhan, N.; Palaninathan, V.; Raveendran, S.; Poulose, A. C.; Nakajima, Y.; Hasumura, T.; Uchida, T.; Hanajiri, T.; Maekawa, T.; Kumar, D. S. N2-Plasma-Assisted One-Step Alignment and Patterning of Graphene Oxide on a SiO2/Si Substrate Via the Langmuir−Blodgett Technique. *Adv. Mater. Interfaces* **2015**, *2*, 1400515.
(47) Dhakate, S. R.; Chauhan, N.; Sharma, S.; Tawale, J.; Singh, S.; Sahare, P. D.; Mathur, R. B. An Approach to Produce Single and Double Layer Graphene from Re-Exfoliation of Expanded Graphite. *Carbon* **2011**, *49*, 1946−1954.
(48) Rakočević, L.; Simatović, I. S.; Maksić, A.; Rajić, V.; Štrbac, S.; Srejić, I. PtAu Nanoparticles Supported by Reduced Graphene Oxide as a Highly Active Catalyst for Hydrogen Evolution. *Catalysts* **2022**, *12*, 43.
(49) Sridhar, V.; Lee, I.; Chun, H.-H.; Park, H. Hydroquinone as a Single Precursor for Concurrent Reduction and Growth of Carbon Nanotubes on Graphene Oxide. *RSC Adv.* **2015**, *5*, 68270−68275.
(50) Wang, Y. Y.; Ni, Z. H.; Yu, T.; Shen, Z. X.; Wang, H. M.; Wu, Y. H.; Chen, W.; Wee, A. T. S. Raman Studies of Monolayer Graphene: The Substrate Effect. *J. Phys. Chem. C* **2008**, *112*, 10637−10640.
(51) Bartošík, M.; Mach, J.; Piastek, J.; Nezval, D.; Konečný, M.; Švarc, V.; Ensslin, K.; Šikola, T. Mechanism and Suppression of Physisorbed-Water-Caused Hysteresis in Graphene FET Sensors. *ACS Sens.* **2020**, *5*, 2940−2949.
(52) Smith, A. D.; Elgammal, K.; Niklaus, F.; Delin, A.; Fischer, A. C.; Vaziri, S.; Forsberg, F.; Råsander, M.; Hugosson, H.; Bergqvist, L.; Schröder, S.; Kataria, S.; Östling, M.; Lemme, M. C. Resistive Graphene Humidity Sensors with Rapid and Direct Electrical Readout. *Nanoscale* **2015**, *7*, 19099−19109.
(53) Islam, S.; Shukla, S.; Bajpai, V. K.; Han, Y.-K.; Huh, Y. S.; Ghosh, A.; Gandhi, S. Microfluidic-Based Graphene Field Effect Transistor for Femtomolar Detection of Chlorpyrifos. *Sci. Rep.* **2019**, *9*, 276.

https://doi.org/10.1021/acsabm.2c00503
ACS Appl. Bio Mater. 2022, 5, 3563−3572

(54) Jang, Y.; Seo, Y.-M.; Jang, H.-S.; Heo, K.; Whang, D. Performance Improvement of Residue-Free Graphene Field-Effect Transistor Using Au-Assisted Transfer Method. *Sensors* **2021**, *21*, 7262.

https://doi.org/10.1021/acsabm.2c00503
ACS Appl. Bio Mater. 2022, 5, 3563−3572